Agricultural and Forest Meteorology 298–299 (2021) 108293

Contents lists available at ScienceDirect

Agricultural and Forest Meteorology

journal homepage: www.elsevier.com/locate/agrformet

Differential response of rice evapotranspiration to varying patterns of warming

Rangjian Qiu [a,*], Gabriel G. Katul [b], Jintao Wang [c], Junzeng Xu [d], Shaozhong Kang [e], Chunwei Liu [a], Baozhong Zhang [f], Longan Li [a], Edward P. Cajucom [g]

[a] Jiangsu Key Laboratory of Agricultural Meteorology, School of Applied Meteorology, Nanjing University of Information Science and Technology, Nanjing 210044, China
[b] Nicholas School of the Environment, Duke University, Durham, North California 27708, USA
[c] Key Laboratory of Agricultural Water Resources, Center for Agricultural Resources Research, Institute of Genetics and Developmental Biology, Chinese Academy of Sciences, 286 Huaizhong Road, Shijiazhuang 050021, China
[d] College of Water Conservancy and Hydropower Engineering, Hohai University, Nanjing 210098, China
[e] Center for Agricultural Water Research in China, China Agricultural University, Beijing 100083, China
[f] State Key Laboratory of Simulation and Regulation of Water Cycle in River Basin, China Institute of Water Resources and Hydropower Research, Beijing 100038, China
[g] Department of Science and Technology-Philippine Atmospheric, Geophysical and Astronomical Services Administration (DOST-PAGASA), Quezon 1100, Philippines

ARTICLE INFO

Keywords:
Accumulative thermal time
Asymmetric warming
Day-time warming
Night-time warming
Priestley-Taylor model
Phenology

ABSTRACT

Rice is a staple food crop that provides more calories to the global population than any other crop. Rice production is also a major consumer of fresh-water resources. Hence, changes in rice evapotranspiration (ET_c) due to projected warming patterns is becoming necessary in any management of water resources and food security assessments. Here, air temperature (T_a) measurements from 1003 meteorological stations covering the period from 1967 to 2016 in China, Japan and the Philippines are first used to assess warming trends. Energy fluxes were then assembled so as to evaluate the responses of rice ET_c to various warming trends. A modified Priestley-Taylor formulation was used to interpret ET_c under differing warming scenarios. Results showed that the average values of daily mean T_a from 1997–2016 increased by 4.6% relative to the period from 1967–1996, where 85% of all stations marked an increase of 0.5–1.5 °C. Greater increment in average daily minima in T_a (5.1%) was noted in the past 20 years compared to the average daily maximum in T_a (3.7%), showing asymmetric warming. The changed growth duration linearly decreased as ambient seasonal mean T_a increased, and higher temperature sensitivity of altered growth duration occurred at greater warming level. Overall, the proposed modified Priestley-Taylor model can be used for estimating ET_c of rice for both half-hourly and daily scales provided the growth duration is a priori known. Changes in seasonal ET_c of rice under varying types of warming patterns are largely explained by both ambient seasonal mean T_a and changes in growth duration.

1. Introduction

Rice (*Oryza sativa* L.), an important staple food, is widely planted worldwide with total planting area over 167 million ha in 2018 (FAO, 2020). It provides food for >50% of the global population, where >90% of the rice is produced and consumed in Asia (Dong et al., 2011; Seck et al., 2012; FAO, 2020). With a growing population worldwide, a 70% increase in food production is necessary to meet projected caloric demands in 2050 (Alexandratos and Bruinsma, 2012). Hence, any reduction in rice production will have adverse impacts on food security (Godfray et al., 2010; Wang et al., 2019). Rice production is facing challenges from numerous factors such as global warming, water shortages, biotic and abiotic stresses, among others that limit the expansion of rice planting area (Peng et al., 2004; Tao et al., 2008). Among these factors, uptick in warming on rice production is of primary concern and continues to draw research attention. Global average surface air temperature was shown to have increased by 0.65–1.06 °C since the pre-industrial times, and is projected to increase further with 1.0 to 3.7 °C by the end of this century (IPCC, 2014). Furthermore, a faster increase in daily minimum temperature was also observed when compared to daily maximum (Peng et al., 2004; Chen et al., 2017). Warming level at different times of the day (i.e. all-day, day-time only, night-time only and asymmetric warming) should have variable effects on rice water consumption, which in turn, affects rice growth and

* Corresponding author.
E-mail address: qiurj@nuist.edu.cn (R. Qiu).

https://doi.org/10.1016/j.agrformet.2020.108293
Received 25 June 2020; Received in revised form 14 December 2020; Accepted 16 December 2020

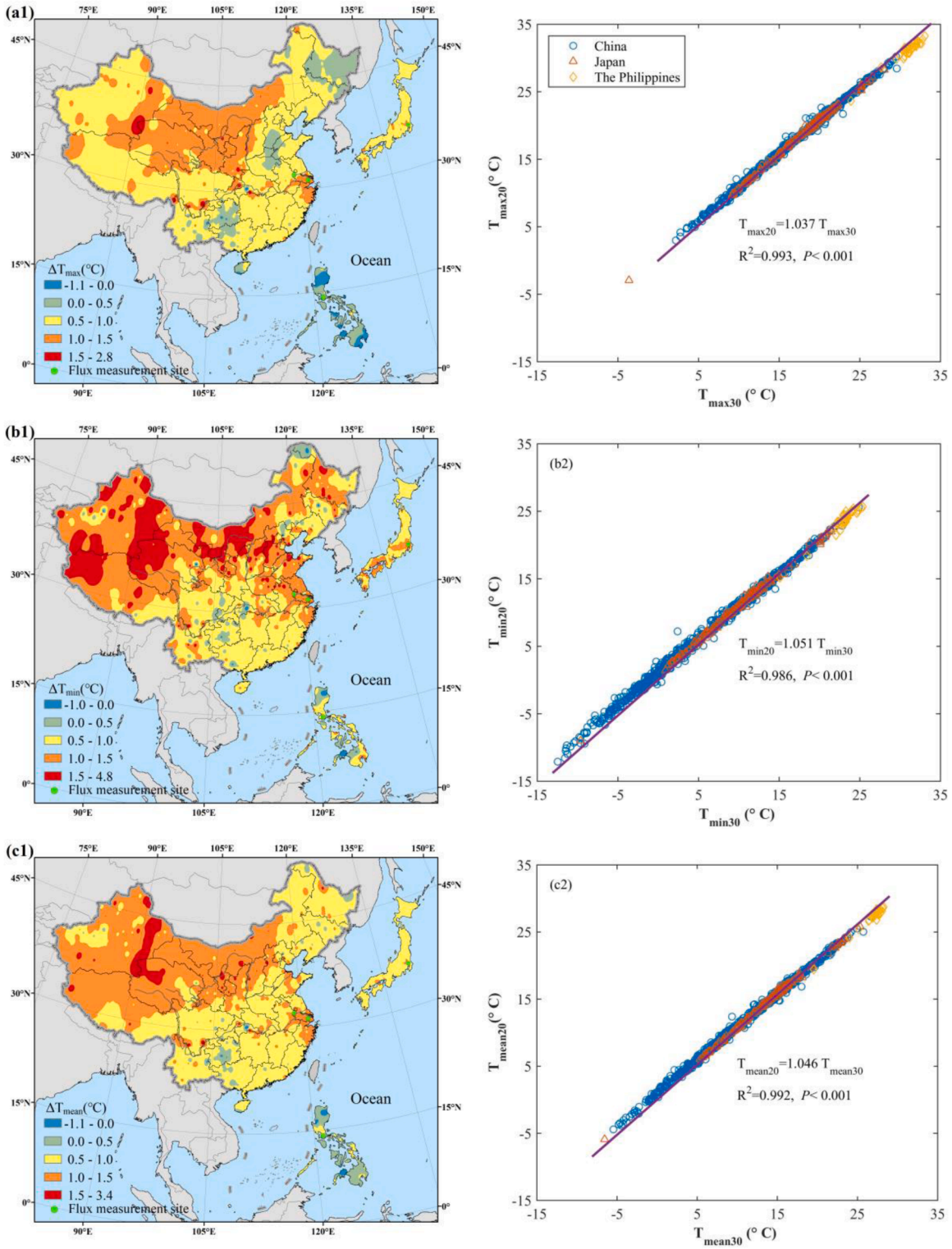

Fig. 1.. Changes in average values of maximum, minimum and mean temperature (ΔT_{max}, ΔT_{min}, ΔT_{mean}) over 1997–2016 relative to 1967–1996 (a1, b1, c1), and relations between average maximum, minimum and mean air temperature over 1997–2016 (T_{max20}, T_{min20}, T_{mean20}) and those over 1966–1996 (T_{max30}, T_{min30}, T_{mean30}) (a2, b2, c2) in China, Japan and the Philippines. The datasets were from 805 meteorological stations in mainland China, 158 stations in Japan and 40 stations in the Philippines. The four flux measurement sites were also marked in the figure.

production.

Controlled manipulation studies such as the Free Air CO_2 Enrichment (FACE) experiments, Open Top Chamber (OTC) experiments, or free air temperature increase facilities experiments have been used to explore varying environmental conditions on rice production (Dong et al., 2011; Cai et al., 2016; Chen et al., 2017; Wang et al., 2018). In these studies, net CO_2 assimilation, crop growth, grain yield and quality have been documented. However, the effects of varying warming patterns on rice evapotranspiration (ET_c) have rarely been reported, which may be attributed to the difficulty in measuring rice ET_c under field condition.

Table 1.
Detailed information on the four rice paddy sites measuring latent heat fluxes

	Site Nanjing	Kunshan	Mase	IRRI
Site characteristics				
Country	China	China	Japan	The Philippines
Position	32.21°N, 118.68°E, altitude 14.4 m	31.25°N, 120.95°E, altitude 17.5 m	36.05°N, 140.03°E, altitude 13 m	14.14°N, 121.26°E, altitude 21 m
Mean annual precipitation (mm)	1106	1100	1200	2075
Mean annual temperature (°C)	15.4	15.5	13.7	27.5
Soil properties				
Soil type	Silt loam	Clay	Clay loam	Silt clay
Bulk density (g cm^{-3})	1.53	1.30	1.35	1.16
Sand-silt-clay (%)	4.6-83.0-12.4	8.9-16.1-75.0	37.5-29.0-33.5	23-45-32
Saturated water content (cm^3 cm^{-3})	0.43	0.50	0.43[a]	0.45[a]
Wilting point (cm^3 cm^{-3})	0.06	0.18	0.08[a]	0.08[a]
Crops/management properties				
Cultivar	Nanjing 5055	Jia 04-33	Koshihikari	NSIC Rc 122
Cropping pattern	Rice - wheat rotation	Rice - wheat rotation	Single rice	Double rice
Planting area (m^2)	210 × 100	200 × 150	1000 × 1500	200 × 200
Start-end of season	Jun. 1–Nov. 8, 2018 May 30–Oct.25, 2019	Jun. 26–Oct. 25, 2013 Jun. 28–Oct. 27, 2014	May 2–Sept. 19, 2002 May 2–Sept. 19, 2003 May 2–Sept. 9, 2004 May 2–Sept. 13, 2005 May 2–Sept. 20, 2006	Dec. 21, 2012–Apr. 1, 2013 Jun. 28–Oct. 22, 2013 Dec. 2, 2013–Mar. 14, 2014 Jun. 18–Oct. 1, 2013
Flooding periods	Most of growth season [b]	Minority of growth season [c]	Most of growth season [d]	Most of growth season [e]
References	Qiu et al. (2019)	Xu et al. (2017a, b; 2019)	Saito et al. (2005); Ono et al. (2015)	Alberto et al. (2009; 2011)

[a] These values were not reported, and were estimated by using a neural network algorithm with the Rosetta package (Schaap, 1999) and reported soil particle data.
[b] Water was drained mostly towards the end of crop development and end of late stages.
[c] The rice field was irrigated following water saving irrigation practice. Under this irrigation practice, the water was absent during most of the period, whereas the rice field was flooded only during the re-green stage or within 3–5 days of fertilizer or pesticide application. The rice field was irrigated to saturated water content when the volumetric soil water content dropped to 60–80% of saturated water content at different growth stages as described elsewhere (Xu et al., 2017b; Liu et al., 2018).
[d] Standing water was covered during transplanting and middle Aug. except for two temporary drainage periods in the middle of the growth season (Saito et al., 2005).
[e] Standing water was absent during 0–37 days after transplanting as well as 1–2 weeks before harvest (Alberto et al., 2011; 2014).

The ET_c is linked to crop growth, biomass and yield production. It is also a primary component in the water and surface energy balance components, and plays an important role in land–atmosphere interaction in the earth system (Koster et al., 2006; Wang and Dickinson, 2012) and in assessment of subsurface processes that are connected to methane and nitrous oxide production. As a result of the large planting area of rice, even small variation in ET_c introduced by global warming can represent substantial volumes of water and may indirectly affect regional climate (Zhang et al., 2019). Unsurprisingly, a quantitative investigation of rice ET_c in response to varying types of warming patterns is becoming necessary for any future water resource management (Pan et al., 2015).

Measurements and observations of rice ET_c in the field under warming conditions face numerous challenges as the paddy rice field is flooded during most of the growing period. Hence, numerical models remain indispensable for estimating rice ET_c into the future. Some studies have used crop models such as CERES-Rice and Oryza 2000 forced by an envelope of climate-change scenarios to estimate the effects of 'all-day' warming on rice ET_c (Tao et al., 2008; Kim et al., 2013). However, uncertainties remain depending on the crop model, the global climate model and emission scenarios used. In addition, crop models running on a daily time scale cannot be used to assess the effect of daytime, nighttime or asymmetric warming on rice ET_c. Furthermore, these crop models require substantial amounts of parameters and parameterization making it difficult to track causal links between warming and responses (such as ET_c). The well-known energy-driven Priestley−Taylor (P−T) model (Priestley and Taylor, 1972), a simplified version of the Penman−Monteith formulation has been widely used and offers a compromise between model complexity and predictive skills. The P−T was shown to reasonably describe hourly or daily ET_c for rice, wheat, maize, cotton, tomato, and mixed land cover types at regional or global scale (Fisher et al., 2008; Yao et al., 2013; Ding et al., 2013a; Ershadi et al., 2014; Ai and Yang, 2016; Qiu et al., 2019 Gong et al., 2021). In this model, ET_c is a product of an equilibrium evaporation rate and a P−T coefficient (α_{PT}), where equilibrium evaporation only depends on meteorological conditions including net radiation, ground soil or water surface heat flux and air temperature. However, the α_{PT} (=1.26) requires modifications for crops even for well-irrigated conditions. The factors affecting α_{PT} reported in the literature include air temperature, relative humidity, mulching, soil moisture availability and leaf area index (Ding et al., 2013a). The leaf area index (highly dynamic for numerous crops) in the proposed model affects the proportional energy received by the canopy and the soil (or water) surface. However, isolating warming effects on leaf area remain fraught with challenges and difficulties. Leaf area dynamics are governed by numerous phenomena including photosynthesis and carbon allocation, phloem transport, nutrient uptake and storage, plant-plant competition for above or below-ground resources, among others. If leaf area can be substituted by a variable that is impacted by temperature, the model may still be used to assess rice ET_c in response to varying types of warming patterns and this frames the scope here.

Warming also impacts phenology, which affects seasonal ET_c. The variation in phenology, mainly due to temperature accumulation, can be described using various temperature response curves based on three cardinal temperatures (Wang and Engel, 1998; Zheng et al., 2014; Aslam et al., 2017). In contrast to prior studies, the Wang–Engel curvilinear temperature response function (Wang et al., 2017a) is introduced here into seasonal ET_c estimates. This function was shown to be reasonably accurate for several crop studies, including rice.

Based on an extensive dataset from 1003 surface meteorological stations distributed in East and Southeast Asia, we first ask whether varying types of warming patterns are evident in the recent 20 years when compared to an earlier 30−year period. A modified P−T model for

estimating half-hourly or daily rice ET_c based on another data set collected from four paddy sites are used to explore schemes linking rice ET_c to temperature. Furthermore, the P−T model is employed to assess the effects of varying types of warming (i.e. all-day, day-time, night-time and asymmetric warming) on rice ET_c considering the varied phenology introduced and documented by warming studies at the four aforementioned sites and others.

2. Materials and methods

2.1. Datasets on temperature collected from meteorological stations

Three datasets were used here. The first dataset includes continuous daily values of maximum, minimum and mean air temperature (T_{max}, T_{min}, and T_{mean}) from 1967 to 2016. The data were provided by 805 surface meteorological stations in mainland China, which were shared freely for teaching and research purposes from the China Meteorological Administration (http://data.cma.cn). The latter two meteorological datasets include continuous monthly T_{max}, T_{min}, and T_{mean} from 1967 to 2016 at 158 stations in Japan and 40 stations in the Philippines. The dataset in Japan, accessed on May 3, 2020, are public and can be downloaded from the Japan Meteorological Agency websites (http://www.jma.go.jp/jma/index.html), while the dataset in the Philippines can be obtained freely for students/academic research purposes following a request from the Philippine Atmospheric, Geophysical, and Astronomical Services Administration websites (DOST-PAGASA) (http://bagong.pagasa.dost.gov.ph/).

The datasets were divided into two time periods 1967–1996 and 1997–2016. These two periods were used to investigate long-term (or climatic) changes in T_{max}, T_{min}, and T_{mean} over the recent 20 years (1997–2016) relative to the previous 30 years (1967–1996).

2.2. Datasets on energy fluxes collected from four paddy sites

Energy fluxes from four paddy rice flux sites in East and Southeast Asia have been collected and analyzed so as to determine ET_c and its relation with warming patterns. These sites include the Nanjing and Kunshan sites in southeast China, the Mase site in Japan, and the International Rice Research Institute (IRRI) site in the Philippines as shown in Fig. 1. The datasets from the Mase and IRRI sites, accessed on July 22, 2019, are public and can be downloaded from the AsiaFlux websites (https://db.cger.nies.go.jp/asiafluxdb/?page_id=16). The detailed site characteristics, soil, crops and management properties are summarized in Table 1.

At the Nanjing site, the half-hourly energy fluxes over the paddy rice field were measured using the Bowen-ratio energy balance method. Detailed information about these energy flux measurements, quality controls, and gap filling procedures are described elsewhere (Qiu et al., 2019). Briefly, the net radiation (R_n, W m^{-2}) and solar radiation (R_s, W m^{-2}) were measured at 2.0 m above the ground by using a NR Lite2 net radiometer (Kipp & Zonen, Delft, Netherlands) and a CS320 digital thermopile pyranometer (Campbell Scientific, Logan, UT, USA), respectively. Air temperature (T_a, °C) and relative humidity (RH, %) were measured at 1.5 m and 2.9 m above the ground using two 083E-1 temperature–humidity probes (Met One Instruments, Grants Pass, OR, USA). A CS451 pressure transducer (Campbell Scientific, Logan, UT, USA) was used to measure surface water level. Volumetric soil water content (θ, cm^3 cm^{-3}) was measured using CS616 water content reflectometers (Campbell Scientific, Logan, UT, USA) at depths from 0.1–0.5 m below the surface at 0.1 m intervals. A SI-111 infrared radiation pyrometer (Apogee Instruments, Logan, UT, USA) oriented vertically downward at a height of 0.1 m above the ground was used to measure the surface or soil water temperature. Two HFP01 heat flux plates (Hukseflux, Delft, Netherlands) buried at a depth of 0.05 m below the ground were used to measure soil heat flux (G_s, W m^{-2}). Four Type-T thermocouples (Omega Engineering, Stamford, CT, USA) were installed to measure soil temperature at soil surface and at a depth of 0.03 m below the ground in line with each soil heat flux plate. All raw data were collected by a CR1000 data logger (Campbell Scientific, Logan, UT, USA) every 5 s and 30-min averages were calculated and stored.

At the Kunshan, Mase and IRRI sites, the half-hourly energy flux data were measured using an open-path eddy covariance system described elsewhere (Saito et al., 2005; Alberto et al., 2012; 2014; Ono et al., 2015; Xu et al., 2017a). Briefly, the latent (λET_c, W m^{-2}) and sensible heat (H, W m^{-2}) fluxes were measured by a triaxial sonic anemometer (model CSAT3; Campbell Scientific, Logan, UT, USA, for the Kunshan and IRRI sites, and model DA-600-3TV; Kaijo, Tokyo, Japan, for the Mase site) and an open path-infrared gas analyzer (model EC150; Campbell Scientific, Logan, UT, USA, for the Kunshan site, and model LI-7500; LI-COR, Lincoln, NE, USA, for the Mase and IRRI sites) operating at a sampling frequency of 10 Hz. Both sensors were installed at 2.5, 3.0 and 2.12 m above the ground, respectively, for the Kunshan, Mase and IRRI sites. The R_n and R_s were measured using a 4-component net radiometer (model CNR4, CNR1; Kipp & Zonen, Delft, Netherlands, and model NR01; Hukseflux, Delft, Netherlands, respectively) at 1.50, 2.35 and 2.79 m above the ground, respectively for the Kunshan, Mase and IRRI sites. The soil heat flux plates (model HFP01; Hukseflux, Delft, Netherlands, or model MF-81; EKO, Tokyo, Japan) were positioned at a depth of 0.05–0.08 m beneath the ground to measure G_s. The θ was measured using time or frequency domain reflectometers (model CS616 or TDR 100; Campbell Scientific, Logan, UT, USA) at soil depths of 0.1, 0.2 and 0.3 m for the Kunshan site, 0.05, 0.1 and 0.2 m for the Mase site and 0–0.25 m for the IRRI site. The soil temperature in the top 0.01-0.40 m soil was measured by TCAV soil thermocouple probes (Campbell Scientific, Logan, UT, USA) at the Kunshan site or Type-T thermocouples (Omega Engineering, Stamford, CT, USA) at the Mase and IRRI sites. All the data were collected by a data logger (model CR5000, CR3000; Campbell Scientific, Logan, UT, USA, or model DRM3; TEAC, Tokyo, Japan) and 30-min averages were calculated and stored. The energy fluxes in these three sites were quality controlled as reported elsewhere (Alberto et al., 2009; Ono et al., 2015; Xu et al., 2017a). The missing half-hourly λET_c and H data were gap-filled using linear regressions between half-hourly λET_c or H and available energy every 14 days for each season. The energy fluxes measured by the eddy covariance system were adjusted by the Bowen-ratio closure method (Twine et al., 2000; Ding et al., 2010). In this method, the Bowen ratio measured by eddy covariance system is assumed to be correct, and this Bowen ratio is employed in the energy-balance closure. Valid objections against using such a correction may be justified as entrainment of heat and water vapor may impact sensible and latent heat fluxes differently; yet these corrections were deemed necessary for uniform comparison across sites and methods. Specifically, the P−T is an energy-based scheme and thus ensuring an energy balance closure in the measurements is recommended for across site comparisons.

For the four sites, the surface soil heat flux (G, W m^{-2}), sum of G_s, heat storage in the soil above the soil heat flux plates and heat storage in the floodwater, was calculated as described elsewhere (Ding et al., 2010; Alberto et al., 2011; Qiu et al., 2019). The heat storage in the floodwater at the Kunshan site was not calculated as a result of the water saving irrigation practices (Table 1) that standing water was absent during most of growth period.

In addition, the fraction of canopy cover (f_c) at the Nanjing site was determined based on eight images of plant canopy using a digital camera at intervals of 7-15 days. The images were analyzed by the CAN-EYE software (V6.1, INRA) that calculates the ratio of green vegetation pixels to the whole image (Liu et al., 2013).

2.3. The modified P−T model

The λET_c (energy flux form) or ET_c (mass flux form) can be estimated using a modified P−T equation (Priestley and Taylor, 1972)

$$\lambda ET_c = \alpha_{PT}\frac{\Delta}{\Delta+\gamma}(R_n - G), \tag{1}$$

where α_{PT} is the bulk P−T coefficient, λ is the latent heat for vaporization (MJ kg^{-1}), γ is the psychrometric constant (kPa °C^{-1}) - almost a constant at a specified site; Δ is the slope of saturation vapour pressure-temperature curve (kPa °C^{-1}) and varies with T_a using (Allen et al., 1998)

$$\Delta = 4098\frac{0.6108\exp(17.27T_a/(T_a+237.3))}{(237.3+T_a)^2}. \tag{2}$$

The λET_c can be divided into its two component λT_r (energy flux form of transpiration) and λE_w (energy flux form of ground evaporation), determined from

$$\lambda T_r = f_t f_{cw}\alpha_{co}\frac{\Delta}{\Delta+\gamma}R_{nc}, \tag{3}$$

$$\lambda E_w = f_{sw}\alpha_{so}\frac{\Delta}{\Delta+\gamma}(R_{nw} - G), \tag{4}$$

where T_r and E_w are the crop transpiration and evaporation, respectively; f_t is the plant temperature constraint; f_{sw} and f_{cw} are the soil moisture constraint for λE_w and λT_r, respectively; R_{nc} is the absorbed energy by the canopy, and R_{nw} is the absorbed energy by water or soil surface. R_{nc} and R_{nw} are given by

$$R_{nc} = (1-\tau)R_n, \tag{5}$$

$$R_{nw} = \tau R_n\ , \tag{6}$$

where τ is the fraction of radiation transmission reaching the water or soil surface, determined as

$$\tau = 1 - f_c^{\beta}, \tag{7}$$

or

$$\tau = exp(-k\mathrm{LAI}), \tag{8}$$

where f_c is the fractional canopy cover [0-1], k is the canopy extinction coefficient set to 0.45 for rice Alberto et al., 2014; Qiu et al., 2019), LAI is the leaf area index, β is a fitting parameter taken as 1.25 for rice based on regression analysis between Eqs. (7) and ((8). The f_c in Eq. (7) is affected by T_a as discussed later that then make it possible to assess the effects of warming on ET_c. The soil moisture constraint for λE_w, f_{sw}, is given as (Ding et al., 2013a)

$$f_{sw} = \begin{cases} S_e S_e < 0.75 \\ 1.0\ S_e \geq 0.75 \end{cases}, \tag{9}$$

where S_e is the effective surface saturation in the 0–0.10 m soil layer, determined as

$$S_e = (\theta - \theta_w)/(\theta_s - \theta_w), \tag{10}$$

where θ_s and θ_w are the volumetric saturated water content and wilting point, respectively (cm^3 cm^{-3}). The plant temperature constraint, f_t, is given by (Yao et al., 2013; Ershadi et al., 2014)

$$f_t = \exp\left(-\left(\frac{T_a - T_{g\ \mathrm{opt}}}{T_{g\ \mathrm{opt}}}\right)^2\right), \tag{11}$$

where $T_{g\ \mathrm{opt}}$ is the optimum plant growth temperature (°C). Based on a meta-data analysis, Sánchez et al. (2014) showed that mean $T_{g\ \mathrm{opt}}$ for *Oryza sativa* is 27.6 °C, which is adopted here. The soil moisture constraint for λT_r, f_{cw}, can be calculated as (Lv et al., 2018)

$$f_{cw} = \begin{cases} 1 & \theta_r \geq \theta_{r1} \\ \ln(1+100\theta_r)/ln(96) & \theta_{r2} < \theta_r < \theta_{r1} \\ 0.963\exp((\theta_r - \theta_{r2})/\theta_{r2}) & \theta_r \leq \theta_{r2} \end{cases} \tag{12}$$

where θ_r is the relative soil moisture content (i.e. the ratio of θ to θ_s), θ_{r1} (95%) and θ_{r2} (80%) are the two critical values of θ_r. α_{co} and α_{so} are the modified P−T coefficients under energy-limited conditions for canopy and water or soil, respectively, given as (Tanner and Jury, 1976)

$$\alpha_{so} = \begin{cases} 1.0 & \tau \leq \tau_c \\ \alpha_o - \dfrac{(\alpha_o - 1)(1-\tau)}{1-\tau_c} & \tau > \tau_c \end{cases} \tag{13}$$

$$\alpha_{co} = \frac{\alpha_o - \alpha_{so}\tau}{1-\tau}, \tag{14}$$

where α_o is the reference P−T coefficient (=1.26). The τ_c is a critical value of τ, normally set as 0.55 (Morgan et al., 2003; Ding et al., 2013a).

To obtain an analytical expression for α_{PT}, G should be expressed as a fraction of R_{nw}, given as

$$G = f_G R_{nw}, \tag{15}$$

where f_G is the fraction of G to R_{nw}, set to 0.36 for rice on half-hourly time scale based on data discussed here Fig. A1). This value was close to that reported in Ding et al (2013a) in a maize field and Choudhury et al., (1987) in a wheat field. On daily time scale, the daily G is small and can be ignored, resulting in an f_G =0. Combined with Eqs. (1)–((15), the expression for a dynamic α_{PT} can be obtained as

$$\alpha_{\mathrm{PT}} = \frac{f_{sw}\alpha_{so}(1-f_G)\tau + f_t f_{cw}\alpha_{co}(1-\tau)}{1-\tau f_G}. \tag{16}$$

2.4. Calculation of daily thermal time and growth duration

The daily thermal time (DTT, °C d) is calculated based on T_{mean} using three cardinal temperatures, given as

$$K(T) = \begin{cases} \dfrac{2\left(T_{\mathrm{mean}} - T_{gmin}\right)^{\alpha}\left(T_{g\ \mathrm{opt}} - T_{g\min}\right)^{\alpha} - \left(T_{\mathrm{mean}} - T_{gmin}\right)^{2\alpha}}{\left(T_{\mathrm{gopt}} - T_{gmin}\right)^{2\alpha}} & T_{gmin} \leq T_{\mathrm{mean}} \leq T_{gmax} \\ 0 & T_{\mathrm{mean}} > T_{gmax} \text{ or } T_{\mathrm{mean}} < T_{gmin} \end{cases}, \tag{17}$$

$$\alpha = \ln 2/\ln\left(\frac{T_{\mathrm{gmax}} - T_{\mathrm{gmin}}}{T_{\mathrm{gmax}} - T_{g\ \mathrm{opt}}}\right)$$

$$\mathrm{DTT} = K(T)\cdot T_{g\ \mathrm{opt}}$$

where $T_{g\ max}$ and $T_{g\ min}$ are the maximum and minimum T_a for crop growth (°C), taken as 41 and 12 °C for rice (Lu et al., 2008), $K(T)$ is the Wang-Engle curvilinear temperature response curve for phenological development rate (Wang and Engel, 1998; Wang et al., 2017a).

Daily thermal time values are converted into accumulated thermal time (ATT, °C) so as to determine growth duration as common in a number of phenology models (He et al., 2015). We assume that the end of the growing season under varying types of warming patterns in each year should attain the same maximum ATT under ambient conditions.

2.5. Estimation of fraction of canopy cover

The development of f_c is now related to ATT. The f_c can be estimated from a modified logistic function given as (Ma and Zhou, 2013)

$$f_c = \frac{a_1}{1+\exp\left(a_2 + a_3 \times \mathrm{ATT_R} + a_4 \times \mathrm{ATT_R}^2\right)}, \quad (18)$$

where a_1, a_2, a_3, a_4 are the fitted empirical coefficients, $\mathrm{ATT_R}$ is the relative ATT, given as

$$\mathrm{ATT_R} = \begin{cases} \mathrm{ATT_i}/\mathrm{ATT_{max\ A}} & \mathrm{ATT_i} \le \mathrm{ATT_{max\ A}} \\ 1 & \mathrm{ATT_i} > \mathrm{ATT_{maxA}} \end{cases}, \quad (19)$$

where $\mathrm{ATT_i}$ is the ATT at the day i, and $\mathrm{ATT_{max\ A}}$ is the maximum ATT under ambient condition. The peak f_c occurs when $\mathrm{ATT_R} = -a_3 / 2a_4$.

2.6. Warming scenarios

Four different warming scenarios are evaluated and are labeled as follows: all-day warming (+1, +2, +3 °C all-day), day-time warming (+1, +2, +3 °C day-time only), night-time warming (+1, +2, +3 °C night-time only) and asymmetric warming (day-time +1 °C, night-time +3 °C). Daytime was defined based on finite shortwave (half-hourly $R_s >$ 10 W m^{-2}) and the remaining time was night-time.

2.7. Accuracy indicators

Various indicators were used to assess the goodness of fit by comparing observed and estimated values of variables (Todorovic et al., 2013; Qiu et al., 2021; Paredes and Pereira, 2019). Here, we use four standard indicators

$$b = \sum_{i=1}^{n} O_i P_i / \sum_{i=1}^{n} O_i^2, \quad (20)$$

$$\mathrm{R^2} = \frac{\left[\sum_{i=1}^{n}\left(O_i - \overline{O}\right)\left(P_i - \overline{P}\right)\right]^2}{\sum_{i=1}^{n}\left(O_i - \overline{O}\right)^2 \sum_{i=1}^{n}\left(P_i - \overline{P}\right)^2}, \quad (21)$$

$$\mathrm{RMSE} = \left[\frac{1}{n}\sum_{i=1}^{n}(P_i - O_i)^2\right]^{0.5}, \quad (22)$$

$$d_{IA} = 1 - \frac{\sum_{i=1}^{N}(Q_i - P_i)^2}{\sum_{i=1}^{N}\left(\left|P_i - \overline{Q}\right| + \left|O_i - \overline{Q}\right|\right)^2}, \quad (23)$$

where O_i and P_i are the observed and estimated values, $\overline{O}$ and $\overline{P}$ are the average observed and estimated values. The b and $\mathrm{R^2}$ are the regression coefficient and the coefficient of determination of the linear regression function forced through the origin (i.e. Y = b X). The RMSE is the root mean squared error. The d_{IA} is the index of agreement. A perfect performance (i.e. model identical to observed) yields b, $\mathrm{R^2}$ and $\mathrm{d_{IA}}$ close to 1.0 and RMSE close to 0 (Qiu et al., 2015).

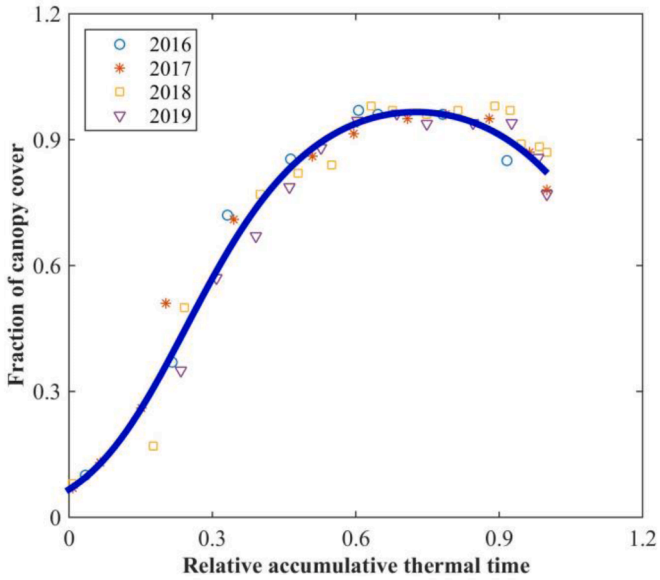

Fig. 2.. The correlation between fraction of canopy cover (f_c) and relative accumulative thermal time ($\mathrm{ATT_R}$) for rice. The regression function was $f_c = 1.24/(1+\exp(2.871 - 11.375\mathrm{ATT_R} + 7.832\mathrm{ATT_R}^2))$ with a coefficient of determination $R^2 = 0.97$ based on the pooled data from Nanjing during 2016 and 2019.

3. Results

3.1. Temperature trends in China, Japan and the Philippines

The 1003 meteorological stations (805 in China, 158 in Japan and 40 in the Philippines) were used to analyze variations in air temperature over the recent 20 years (1997–2016) relative to an earlier 30 years (1967–1996). Overall, the increases in daily $\mathrm{T_{max}}$, $\mathrm{T_{min}}$ and $\mathrm{T_{mean}}$ over the recent 20 years was apparent in 99.3% (799), 98.0% (789) and 98.9% (796) of the stations, respectively, in China, in 99.4% (157), 98.7% (156) and 100% (158) of the stations, respectively in Japan and 62.5% (25), 92.5% (37) and 87.5% (35) of the stations, respectively in the Philippines. On average, the average values of daily $\mathrm{T_{max}}$, $\mathrm{T_{min}}$ and $\mathrm{T_{mean}}$ over the recent 20 years were increased by 0.80, 1.01 and 0.85 °C, respectively for China, 0.80, 0.88 and 0.78 °C, respectively for Japan and 0.18, 0.65 and 0.41 °C, respectively for the Philippines. The spatial distribution of varying levels of changes in air temperature were also analyzed and shown in Fig. 1. The increment in average daily $\mathrm{T_{max}}$ over the recent 20 years was mainly concentrated in 0.5–1.0 °C range for China and Japan (60.1% of total in China, 77.2% in Japan), while in the 0–0.5 °C range for the Philippines (42.5%). The average values of daily $\mathrm{T_{min}}$ increased by 0.5–1.0 °C and 1.0–1.5 °C, respectively, for 43.1% and 30.6% of total stations (Fig. 1 b1) in China, 57.6% and 29.7% of total in Japan, and 35.0% and 22.5% of stations in the Philippines. Interestingly, the greater increment of average values of daily $\mathrm{T_{min}}$ (i.e. >1.5 °C), mainly distributed in Northern China, accounted for 15.2% of the total stations in China. Regression analysis also showed that the increment of average values of daily $\mathrm{T_{min}}$ (5.1%) over the recent 20 years was greater than that of daily $\mathrm{T_{max}}$ (3.7%) (Fig. 1 a2, b2), indicating faster night-time warming than day-time warming in these countries. The average values of daily $\mathrm{T_{mean}}$ over the recent 20 years across all stations increased by 4.6% (Fig. 1 c2) where 85% of stations recorded an increase by 0.5–1.5 °C (Fig. 1 c1). All in all, these results show that warming trends were asymmetric (night-time warming exceeding day-time).

3.2. Dynamics of f_c under varying warming trends

The relation between f_c and ATT was analyzed based on the pooled

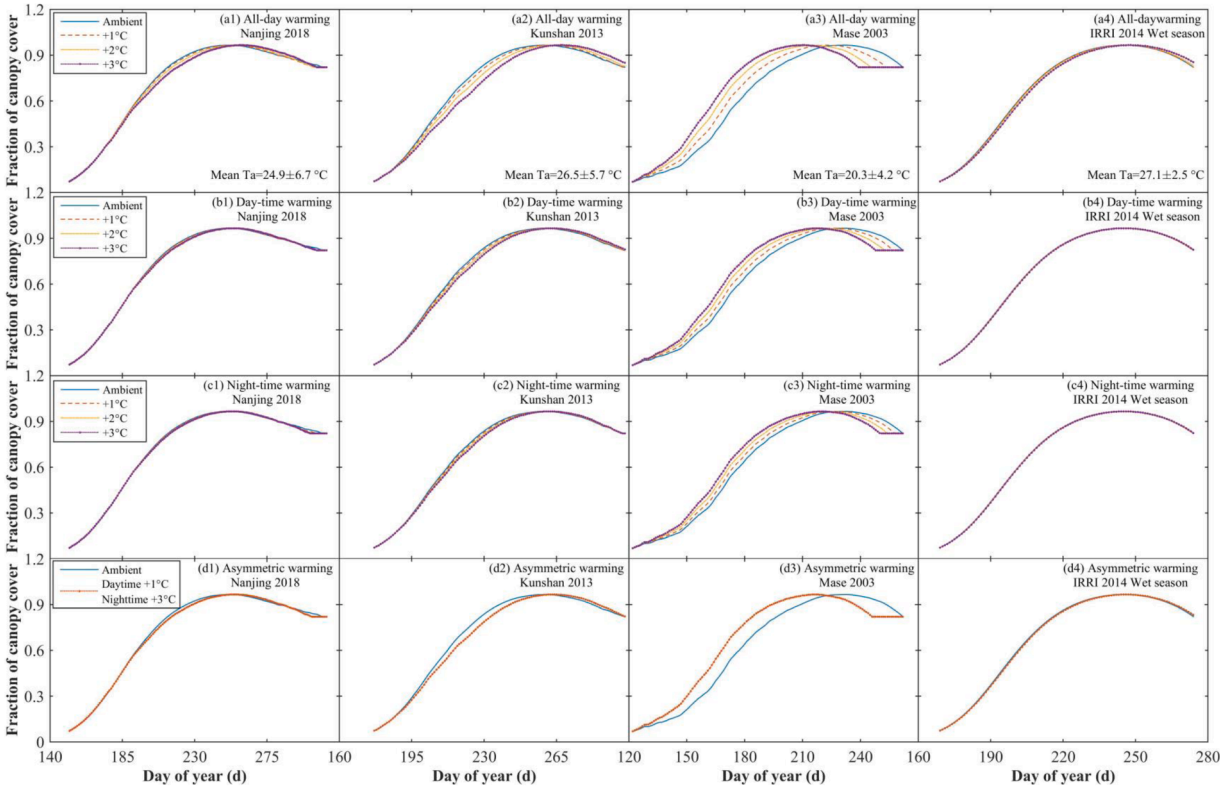

Fig. 3.. Responses of fraction of canopy cover to all-day (a1-a4), day-time (b1-b4), night-time (c1-c4) and asymmetric warming (d1-d4) in 2018 at the Nanjing site (a1-d1), 2013 at the Kunshan (a2-d2) and the Mase sites (a3-d3) and wet season in 2014 at the IRRI site (a4-d4).

Table 2.
The variation of growth duration under all-day, day-time, night-time and asymmetric warming. T_a is air temperature. DTT is the daily thermal time. $ATT_{max\ A}$ is the maximum accumulative thermal time under ambient condition. DS and WS are the dry- and wet- season, respectively, in the Philippines.

Site	Season	Days	Seasonal mean T_a (°C)	Mean DTT (°C d)	$ATT_{max\ A}$ (°C)	Shortened days (d) All-day warming (°C)			Day-time warming (°C)			Night-time warming (°C)			Asymmetric warming (°C)
						+1	+2	+3	+1	+2	+3	+1	+2	+3	Day-time +1Night-time +3
Nanjing	2018	161	24.9±6.7	22.6	3637	5	6	3	2	3	3	3	6	7	7
	2019	149	24.9±5.3	24.3	3626	5	6	5	3	4	5	3	5	7	7
Kunshan	2013	122	26.5±5.7	24.0	2930	0	-2	-[a]	0	-1	-[a]	1	1	1	-1
	2014	122	24.3±3.7	24.4	2981	4	6	7	2	4	5	2	5	6	7
Mase	2002	141	22.0±5.1	21.1	2976	8	13	16	5	8	11	4	7	10	13
	2003	141	20.3±4.2	19.3	2722	8	16	23	5	9	14	4	8	11	16
	2004	131	22.7±5.2	22.3	2916	4	8	11	2	5	7	2	4	6	8
	2005	135	21.8±2.2	21.0	2838	6	11	14	3	7	10	2	5	7	10
	2006	142	21.5±4.4	21.2	3008	8	14	18	4	9	12	3	8	11	13
IRRI	2013 DS	102	25.7±2.2	27.0	2750	1	1	1	1	1	1	0	1	1	1
	2013 WS	117	26.6±2.3	27.4	3201	0	-1	-2	0	0	0	0	0	0	-1
	2014 DS	103	24.8±2.5	26.3	2709	2	3	3	1	2	2	1	2	3	3
	2014 WS	106	27.1±2.5	27.4	2909	0	-1	-4	0	0	-1	0	0	-1	-2

[a] The data after 3 days of end of season are unavailable.

data from the Nanjing site since the f_c data were not available at other sites. The dynamics of f_c was related to the relative ATT. Fig. 2 shows that the f_c in 2018 and 2019 increased rapidly as relative ATT increased until it reached about 0.73, followed by a gradual decline. Independent data in 2016 and 2017 at the Nanjing site are also included in Fig. 2 for reference and show analogous variation. This trend between f_c and relative ATT could be captured by the modified logistic function (Fig. 2). The b between observed and estimated f_c was 0.996, and the R^2, RMSE and d_{IA} were 0.97, 0.05 and 0.993, respectively. These statistical indicators suggest that the modified logistic function for estimating f_c was reasonable and can be used to represent the dynamics of f_c when daily T_a during the growth period is known. Using relative ATT rather than ATT here can reduce bias in f_c produced by ATT differences across regions.

The effects of varying trends in warming on the dynamics of f_c are presented in Fig. 3, where the specified year at each site was selected for reference (i.e. in 2018 at the Nanjing site, 2013 at the Kunshan site, 2003 at the Mase site, 2014 wet season at the IRRI site). The differential responses of dynamic f_c to the four warming scenarios are now compared. At the Nanjing and Kunshan sites, the development of canopy cover for all four types of warming scenarios was slower than under ambient

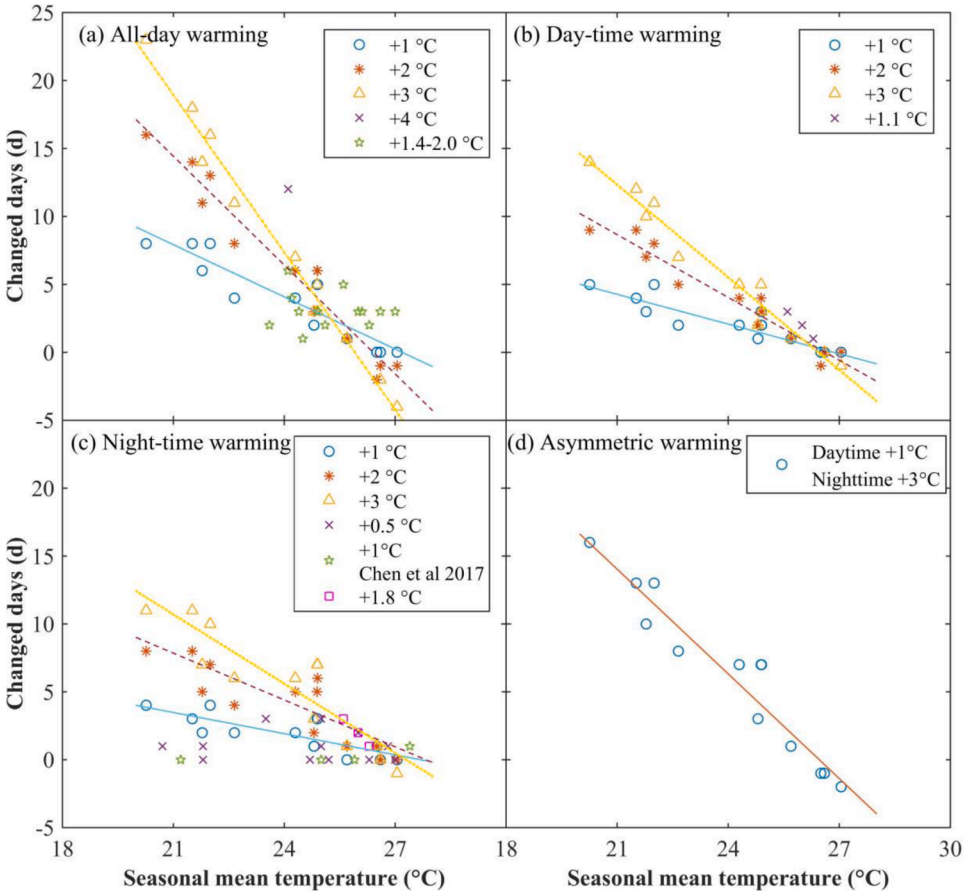

Fig. 4.. The relation between shortened growth duration and seasonal mean temperature under varying types of warming (all-day, day-time, night-time and asymmetric). The dataset for all-day warming by 1.4–2.0 °C and 4 °C (Dong et al., 2011; Rani and Maragatham, 2013; Cai et al., 2016; Wang et al., 2018), day-time warming by 1.1 °C (Dong et al., 2011) and night-time warming by 0.5–1.8 °C (Dong et al., 2011; Chen et al., 2017) were included for reference. The data without significant difference among treatments in the literature were set to be identical.

Table 3.
The regression functions between the shortened days and ambient seasonal mean temperature under different types of warming (all-day, day-time, night-time and asymmetric). The data are shown in Fig. 4.

Warming type	Level (°C)	Regression functions	N	R^2
All-day	+1	y=-1.28x+34.8	13	0.83***
	+2	y=-2.67x+70.3	13	0.95***
	+3	y=-3.86x+99.9	12	0.98***
Day-time	+1	y=-0.73x+19.7	13	0.82***
	+2	y=-1.54x+40.9	13	0.94***
	+3	y=-2.27x+59.9	13	0.96***
Night-time	+1	y=-0.52x+14.3	13	0.62**
	+2	y=-1.15x+31.6	13	0.75***
	+3	y=-1.70x+46.2	12	0.82***
Asymmetric	Day-time +1, Night-time +3	y=-2.56x+67.9	13	0.92***

** and *** indicate the significant level at $P < 0.01$ and 0.001.

condition (Fig. 3 a1-d1, a2-d2), and greater variations in f_c were observed for the Kunshan site in 2013 than the Nanjing site in 2018. Similar trends in f_c induced by warming was also observed at the IRRI site where small variation was noted under all-day warming (Fig. 3 a4), whereas only tiny changes were noted under day-time, night-time and asymmetric warming (Fig. 3 b4-d4). In contrast, the development of canopy coverage under warming was faster than under ambient condition at the Mase site (Fig. 3 a3-d3). Generally, compared to ambient conditions, the largest variations in f_c were observed under all-day warming followed by asymmetric, day-time and night-time warming. All in all, greater warming levels lead to greater variations in f_c.

3.3. Variation of rice growth duration under warming

There are differential responses of growth duration to varying types of warming at the sites (Table 2). All-day warming shortened the growth duration by 3–6 d at the Nanjing site, 4–23 d at the Mase site, 1–3 d for the dry season at the IRRI site, 4–7 d for cool season (2014) at the Kunshan site, while it prolonged the growth duration by 0–4 d for the warm season (2013) at the Kunshan site and wet seasons at the IRRI site. Similar trends were also observed for day-time and night-time warming. The variations of growth duration under asymmetric warming (day-time +1 °C, night-time +3 °C) are similar to the +2 °C all-day warming at all sites. At the Mase site, the end of the growing season was earlier with increasing (all-day, day-time and night-time) warming level, as well as for day-time and night-time warming in 2019 at the Nanjing site, and in 2014 at the Kunshan site. However, greater warming did not always lead to further shortening of growth duration. In the 2013 dry season at the IRRI site, the reduction of growth duration was almost the same under different warming levels (all-day, day-time and night-time), as well as for day-time and night-time warming in the wet season of 2013 at the IRRI site and the night-time warming in 2013 at the Kunshan site. Furthermore, the shortened growth duration remained 'stagnant' or reduced beyond +2 °C warming at the Nanjing site and in the dry season of 2014 at the IRRI site. Increased all-day warming even further postponed the end of the growing season in the warm season (2013) at the Kunshan site and wet season at the IRRI site when the ambient seasonal mean T_a was high.

The variations of growth duration under varying types of warming are related to ambient seasonal mean T_a as shown in Fig. 4 and Table 3. Linear decline curves were found between the changed growth duration and ambient seasonal mean T_a under varying types of warming patterns. Independent data from the literature for rice are also included in Fig. 4

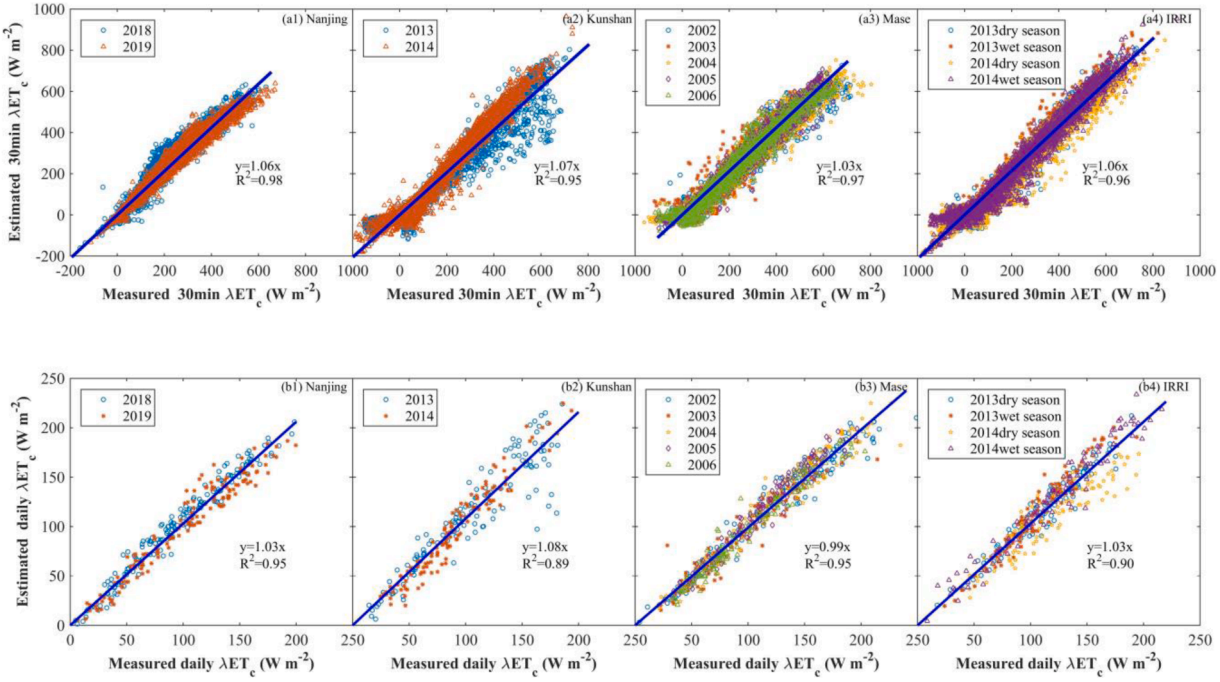

Fig. 5.. Comparison of half-hourly (a1-a4) and daily (b1-b4) latent heat fluxes (λET_c, ET_c is evapotranspiration) measured and estimated by the modified Priestley–Taylor model at the Nanjing (a1, b1), Kunshan (a2, b2), Mase (a3, b3) and IRRI (a4, b4) sites. The blue line in each panel is the fitted line forced through the origin based on the pooled data.

Table 4
The goodness of fit statistical indicators when comparing the half-hourly and daily values of latent heat flux (λET_c, ET_c is evapotranspiration) observed and estimated by the modified Priestley-Taylor model.

Site	Season	30-min λET_c				Daily λET_c			
		b	R^2	RMSE (W m^{-2})	d_{IA}	*b*	R^2	RMSE (W m^{-2})	d_{IA}
Nanjing	2018	1.10	0.97	29.3	0.988	1.06	0.97	10.7	0.987
	2019	1.03	0.98	21.2	0.995	1.00	0.95	10.5	0.986
	Whole data	1.06	0.98	25.6	0.992	1.03	0.95	10.6	0.987
Kunshan	2013	1.03	0.95	39.6	0.986	1.07	0.85	19.3	0.950
	2014	1.14	0.96	35.2	0.982	1.09	0.94	13.3	0.968
	Whole data	1.07	0.95	37.5	0.985	1.08	0.89	16.6	0.959
Mase	2002	1.01	0.97	25.8	0.993	0.98	0.96	10.9	0.989
	2003	1.03	0.95	28.3	0.985	0.97	0.93	10.8	0.980
	2004	1.02	0.98	25.8	0.994	1.01	0.95	10.4	0.988
	2005	1.05	0.98	23.1	0.994	1.03	0.97	8.5	0.988
	2006	1.01	0.97	22.3	0.992	0.97	0.96	8.8	0.989
	Whole data	1.03	0.97	25.1	0.992	0.99	0.95	9.9	0.988
IRRI	2013 dry season	1.08	0.96	31.5	0.987	1.04	0.94	8.5	0.978
	2013 wet season	1.11	0.97	29.6	0.988	1.08	0.94	11.5	0.964
	2014 dry season	0.99	0.95	33.1	0.987	0.92	0.86	13.8	0.948
	2014 wet season	1.07	0.97	31.6	0.989	1.07	0.96	11.6	0.981
	Whole data	1.06	0.96	31.5	0.988	1.03	0.90	11.5	0.970

for reference and support the magnitudes calculated here. The greater temperature sensitivity of changed growth duration was found with greater warming level (Table 3). At a prescribed warming level, the temperature sensitivity was greater in all-day warming, followed by day-time and night-time warming (Table 3, Fig. 4), while the asymmetric warming shows a similar trend to the +2 °C all-day warming.

3.4. Assessing the ET_c of rice estimated by using the modified P−T model

The comparisons between half-hourly or daily observed and modeled ET_c using the modified P−T formulation are shown in Fig. 5. Table 4 summarizes the goodness of fit measures. Generally, the agreement between observed and estimated half-hourly ET_c at all sites is acceptable. The values of *b* were 1.03–1.10, 1.03–1.14, 1.01–1.05 and 0.99–1.11 for the Nanjing, Kunshan, Mase and IRRI sites, respectively, with corresponding R^2 of 0.97–0.98, 0.95–0.96, 0.95–0.98 and 0.95–0.97, indicating that estimated values of half-hourly ET_c are statistically close to the observed ones and most of variation of the estimated values is explained by the modified P−T model. The values of RMSE, which characterizes the variance of the errors, ranged from 21 to 40 W m $^{-2}$ at all sites. The values of d_{IA} were higher than 0.98, suggesting that mean square error is close to the potential.

Daily values of ET_c estimated by the modified P−T model also show good agreement with observations at all sites with *b* of 0.92–1.09, R^2 of 0.85–0.97, RMSE of 8–19 W m $^{-2}$ and d_{IA} of 0.95–0.99 (Table 4, Fig. 5 b1-b4). All in all, these goodness of fit indicators show that the modified P−T model is robust and could be widely used to estimate the ET_c of rice for both half-hourly and daily time scale. Daily ET_c is also reported here because it is essential for developing precision irrigation scheduling (Ding et al., 2013a). To be clear, both data and model are using the same

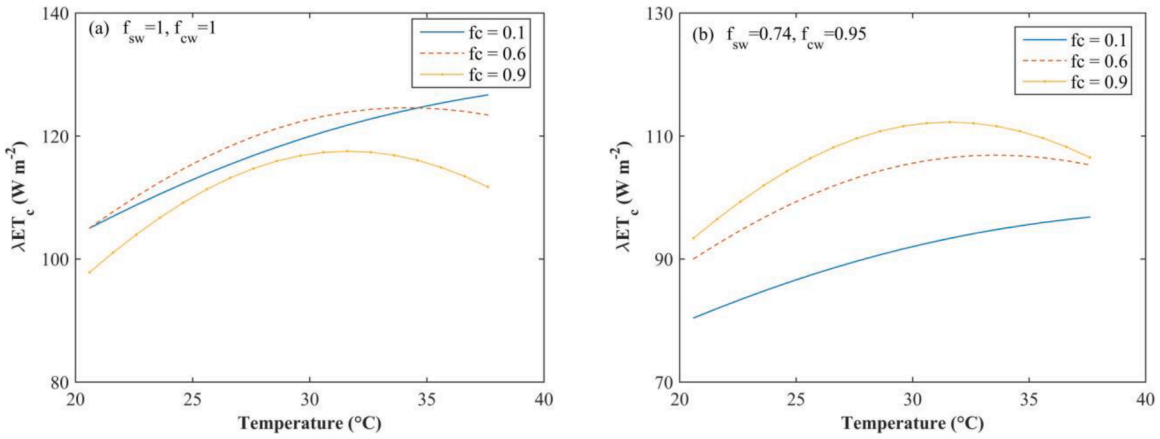

Fig. 6.. The responses of latent heat flux (λET_c, ET_c is evapotranspiration) to air temperature under varying fraction of canopy cover (f_c) without (a) and with (b) soil moisture constraint. The net radiation (R_n) minus surface ground soil flux (G) is set as 120 W m^{-2}. The f_{sw} and f_{cw} are soil moisture constraint for evaporation and transpiration, respectively.

Table 5.
Changes in seasonal evapotranspiration (ET_c) between varying types of warming and ambient condition with or without changed growth duration at all sites. DS and WS are the dry- and wet- season. T_a is air temperature.

	Sites	Season	Seasonal mean T_a (°C)	Seasonal ET_c differences (mm)									
				All-day warming (°C)			Day-time warming (°C)			Night-time warming (°C)			Asymmetric warming (°C)
				+1	+2	+3	+1	+2	+3	+1	+2	+3	Day-time +1 night-time +3
Changed growth duration	Nanjing	2018	24.9	-1.7	-2.3	3.4	2.2	1.9	2.0	-1.4	-5.8	-7.4	-5.2
		2019	24.9	-4.6	-4.9	-1.1	-1.3	0.3	-0.7	-5.3	-8.5	-13.4	-9.8
	Kunshan	2013	26.5	1.6	6.6	- [a]	2.3	5.4	-[a]	-1.5	-2.1	-2.6	2.4
		2014	24.3	-2.9	-3.7	-2.1	2.3	1.3	1.6	-2.9	-10.3	-12.4	-8.7
	Mase	2002	22.0	-12.8	-20.6	-25.8	-4.3	-7.7	-12.7	-9.7	-13.9	-26.9	-25.6
		2003	20.3	-20.7	-44.4	-60.1	-9.6	-18.1	-29.7	-12.6	-28.1	-40.2	-50.6
		2004	22.7	-10.6	-17.0	-25.6	-3.8	-6.4	-8.1	-10.8	-17.6	-20.7	-22.4
		2005	21.8	-12.7	-23.7	-32.4	-2.9	-10.6	-13.9	-7.7	-14.8	-23.8	-24.6
		2006	21.5	-12.4	-22.2	-35.0	-4.1	-8.6	-14.6	-8.3	-18.2	-26.0	-24.7
	IRRI	2013 DS	25.7	-1.6	0.8	2.1	4.7	4.1	7.4	-0.4	-5.6	-5.9	-2.1
		2013 WS	26.6	3.4	9.5	14.9	3.6	6.3	8.3	0.3	0.6	0.8	7.6
		2014 DS	24.8	-4.8	-6.5	-4.2	0.6	0.7	3.9	-4.9	-9.4	-14.4	-10.0
		2014 WS	27.1	2.1	8.1	16.5	3.1	5.5	11.6	0.1	0.2	5.3	10.8
No changed growth duration	Nanjing	2018	24.9	2.8	4.6	5.5	2.5	3.8	4.0	0.3	0.6	0.9	3.5
		2019	24.9	3.6	6.1	7.4	3.9	6.5	7.9	-0.3	-0.5	-0.7	3.2
	Kunshan	2013	26.5	1.6	2.4	2.5	2.3	3.5	3.8	-0.7	-1.3	-1.8	0.6
		2014	24.1	4.6	8.4	11.4	5.0	9.0	12.1	-0.4	-0.7	-0.9	4.1
	Mase	2002	22.0	6.9	12.9	17.9	6.8	12.4	16.9	0.1	0.2	0.3	7.4
		2003	20.3	8.4	16.4	23.6	7.9	15.1	21.6	0.3	0.7	1.2	9.5
		2004	22.7	6.3	11.4	15.2	6.7	12.1	16.0	-0.4	-0.7	-1.0	5.7
		2005	21.8	7.1	13.3	18.5	7.2	13.3	18.3	-0.1	-0.2	-0.3	7.1
		2006	21.5	7.4	14.0	19.7	6.8	12.7	17.5	0.6	1.1	1.7	8.6
	IRRI	2013 DS	25.7	3.4	5.7	7.0	3.7	6.4	8.0	-0.4	-0.7	-0.9	2.8
		2013 WS	26.6	3.4	5.8	7.1	3.1	5.2	6.3	0.3	0.6	0.8	3.9
		2014 DS	24.8	4.2	7.4	9.7	4.4	7.8	10.2	-0.3	-0.5	-0.6	3.8
		2014 WS	27.1	2.1	3.1	3.1	2.0	2.9	2.8	0.1	0.2	0.2	2.3

[a] The data after 3 days of end of this season are unavailable.

measured net radiation, which can explain the high R^2. However, that the b is close to unity and the RMSE is small at diurnal and daily scales also suggest that the P-T coefficient is reasonably reproduced by the proposed model.

3.5. Potential effect of global warming on ET_c of rice

Fig. 6 shows the response of ET_c to T_a under varying f_c. At low f_c, the ET_c of rice almost linearly increased with increasing T_a since evaporation was the dominant proportion of ET_c. While at high f_c, when transpiration was dominant, the ET_c response to T_a showed rapid increases until it reached to 32-34 °C, followed by a gradual decline. A higher f_c also induced a greater reduction rate of ET_c beyond the critical T_a.

At the seasonal scale, the seasonal ET_c considering changed growth duration shows different responses to varying types of warming patterns at different sites, as illustrated in Table 5 and Fig. 7. At the Nanjing site, the seasonal ET_c was reduced for all levels of night-time warming, all-day warming below +3 °C and asymmetric warming, whereas increased for most levels of day-time warming. Similar results were also observed for the Kunshan site. At the Mase site, greater reduction of

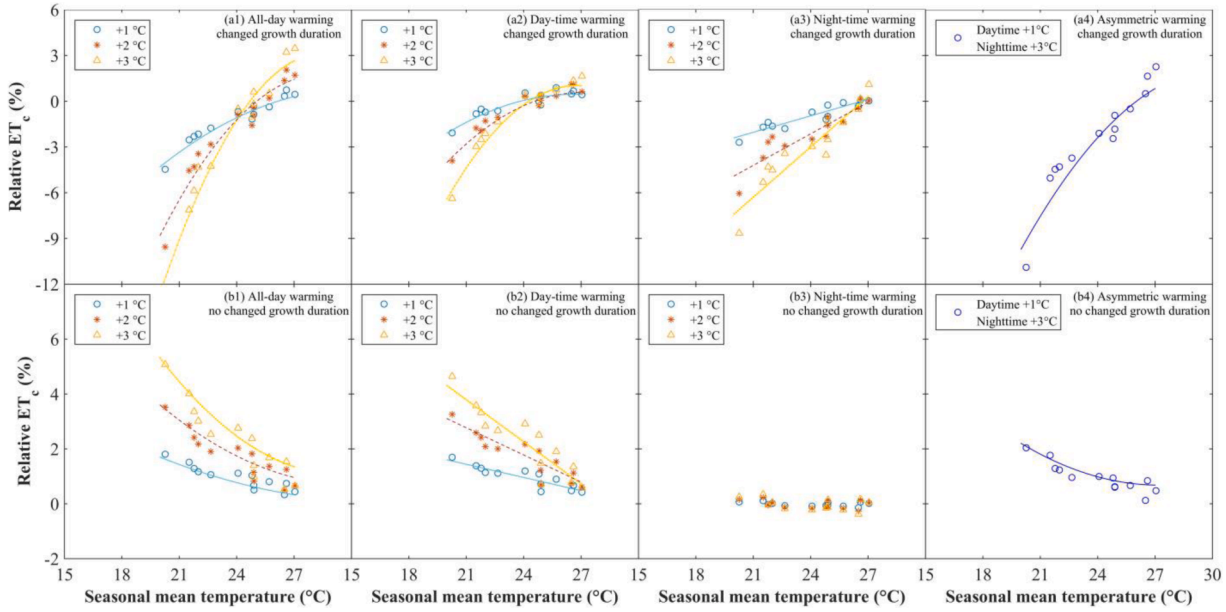

Fig. 7.. The relations between relative seasonal evapotranspiration (($ET_{c\ W}$-$ET_{c\ A}$)/$ET_{c\ A}$), where $ET_{c\ W}$ and $ET_{c\ A}$ are seasonal ET_c under warming and ambient conditions) and seasonal mean temperature under varying types (all-day (a1, b1), day-time (a2, b2), night-time (a3, b3) and asymmetric (a4, b4)) of warming patterns with (a1-a4) or without (b1-b4) considering changed growth duration.

Table 6.
The regression functions between relative changes in seasonal evapotranspiration (($ET_{c\ W}$-$ET_{c\ A}$)/$ET_{c\ A}$), where $ET_{c\ W}$ and $ET_{c\ A}$ are seasonal ET_c under warming and ambient conditions) and ambient seasonal mean temperature with and without changed growth duration under varying types of warming (all-day, day-time, night-time and asymmetric).

Warming type	Levels (°C)	Changed growth duration Regression functions	R^2	No changed growth duration Regression functions	R^2	N
All-day	+1	y=-0.049x^2+2.96x-43.9	0.95***	y=0.012x^2-0.76x+12.1	0.84***	13
	+2	y=-0.144x^2+8.23x-115.8	0.94***	y=0.029x^2-1.74x+26.8	0.85***	13
	+3	y=-0.219x^2+12.47x-174.4	0.92***	y=0.048x^2-2.82x+42.5	0.87***	12
Day-time	+1	y=-0.058x^2+3.09x-40.7	0.87***	y=-0.16x+4.8	0.79***	13
	+2	y=-0.091x^2+4.93x-66.2	0.95***	y=-0.33x+9.7	0.81***	13
	+3	y=-0.160x^2+8.58x-114.0	0.97***	y=-0.51x+14.5	0.82***	12
Night-time	+1	y=0.36x-9.6	0.87***	-	-	-
	+2	y=0.69x-18.7	0.83***	-	-	-
	+3	y=1.10x-29.4	0.89***	-	-	-
Asymmetric	Day-time +1 Night-time +3	y=-0.108x^2+6.58x-98.1	0.90***	y=0.029x^2-1.58x+22.2	0.84***	13

seasonal ET_c was observed under varying types of warming when compared to the other sites, mainly due to shortened growth duration and cooler season (Tables 2 and 4). Compared with ambient conditions, a greater warming level at the Mase site resulted in a greater reduction of seasonal ET_c. Differing warming types also lead to different variations of seasonal ET_c at the Mase site. The greater fluctuations of seasonal ET_c were found under all-day warming, followed by asymmetric, night-time and day-time warming. At the IRRI site, the values of seasonal ET_c were generally increased for different warming patterns except for all-day and night-time warming in some dry seasons, and higher increment appeared under greater warming level.

The relative changes in seasonal ET_c under varying types of warming patterns was related to ambient seasonal mean T_a and can be summarized by a linear (night-time warming) or parabolic (other types of warming) increase curves (Fig. 7, Table 6). The greater temperature sensitivity of relative changed seasonal ET_c was found with greater overall warming level.

If not considering changes to the growth duration, the seasonal ET_c relation appears to be mixed. At a preset warming level, the all-day and day-time warming scenarios generated greater seasonal ET_c than night-time warming, while asymmetric warming resulted in changes similar to seasonal ET_c when the all-day warming level was between +1 and +2 °C. The modified seasonal ET_c without considering alterations to growth duration generated linear (day-time warming) or parabolic (all-day and asymmetric warming) reduction curves pattern in response to ambient seasonal mean T_a (Fig. 7 b1-b4). These results indicate that altered growth duration cannot be ignored when assessing variations of seasonal ET_c with warming.

4. Discussion and conclusions

A modified P−T model was proposed to assess the effects of various warming patterns on rice ET_c at multiple sites in East and Southeast Asia, one of major hubs for rice cultivation (Dong et al., 2011). The model accommodates soil moisture and plant temperature constraints. The main features of the model here, when compared to prior work (Ding et al., 2013a; Qiu et al., 2019), include the usage of f_c instead of LAI. There are many benefits to using f_c. First, f_c can be readily obtained in the field from digital (or phone) camera or even visual inspection (Allen and Pereira, 2009; Ding et al., 2013b). In addition, f_c variations at regional scales may be accessed from remote sensing platforms (Steduto et al., 2009). Furthermore, the development of f_c [0-1] was found to be related to ATT (Fig. 2), which makes it possible to assess global warming on rice ET_c since f_c is the only crop parameter needed in the model.

Table 7.
Summary of model findings for the effects of all-day warming on seasonal evapotranspiration (ET_c) of rice reported in the literature.

Warming level (°C)	Relative changed seasonal ET_c (%)	Changed growth duration?	Crop pattern	Location	Model	Source
+2.08	-7.2~0[a]	Yes	Single rice	Gwangju, Korea	DSSAT4.0-CERES-rice	Kim et al. (2013)
+3.09	-7.5~0[a]	Yes				
+1	-4	Yes	Double rice	Bangladesh	YIELD	Mahmood (1997)
-	Increase	No	-	Indonesia	Energy balance	Saptomo et al. (2009)
+1	-10.7~-3.3	Yes	Single rice (Harbin), rice-wheat rotation (Hefei, Chengdu), double rice (Nanchang, Changsha)	Harbin, Hefei, Chengdu, Nanchang and Changsha in China	DSSAT4.0-CERES-rice	Tao et al. (2008)
+2	-14.3~-4.8	Yes				
+3	-18.2~4.3	Yes				
+1	0	Yes	Early rice	Guangzhou, China		
+2	-1.7	Yes				
+3	-0.37	Yes				
+1	0.5	Yes	Late rice	Guangzhou, China		
+2	0.9	Yes				
+3	5.6	Yes				

[a] All-day warming had significant effect for cultivars Nampyeong and Saekyewha, whereas no significant effect for cultivar Unkwang.

The modified P−T model was evaluated using energy flux datasets from four sites in Asia. Overall results show that the proposed modified P−T model is acceptable for both half-hourly and daily scales at multiple sites (Table 4, Fig. 5). Many studies also indicated that the P−T formulation can estimate ET_c provided adjustments are made to the P−T coefficient for various crops as reported for maize, rice, wheat, tomato, and cotton (Ding et al., 2013a; Ai and Yang, 2016; Qiu et al., 2019; Gong et al., 2021), pasture (Sumner and Jacobs, 2005) and mixed land cover types at regional or global scales using remote sensing (Fisher et al., 2008; Yao et al., 2013; Ershadi et al., 2014). The dynamic α_{PT} in these studies was well described by using a combination of multiplicative functions reflecting limiting factors to water uptake such as soil and plant moisture constraints, plant temperature constraint, green canopy fraction, fraction of ground mulching and relative surface wetness.

The modified P−T model was used here to assess warming patterns on rice ET_c. The parameter f_c in the model was influenced by warming as shown across multiple sites. The responses of a dynamic f_c to varying types of warming patterns at different sites were, however, not identical. At the Nanjing and Kunshan sites, the development of f_c under an all warming pattern were slower than under ambient condition (Fig. 3 a1-d1, a2-d2). An opposite trend at the Mase site (Fig. 3 a3-d3) was found. At the IRRI site, small variations in f_c were observed under varying types of warming relative to ambient condition (Fig. 3 a4-d4). These site differences depend on the ambient seasonal mean T_a and its deviation (Fig. 3), which in turn affects ATT under varying types of warming. The f_c variations are consistent with studies reporting LAI variations with warming. For instance, a FACE experiment showed that a +2.0 °C all-day warming led to significant reductions in LAI by 24%, 17%, 12% and 10%, respectively for the jointing, booting, heading and milking stages of rice in a warm season (2013, seasonal mean T_a of 27.0 ± 4.2 °C), whereas it did not significantly affect LAI in a cool season (2014, seasonal mean T_a of 24.2 ± 3.4 °C) as discussed elsewhere (Cai et al., 2016). Night-time warming by 0.5 °C significantly reduced LAI at the grain filling stage by 7-12% for early and middle rice (seasonal mean T_a of 25.0–27.4 °C), whereas it increased LAI by 44% for single rice with low seasonal mean T_a (20.7–21.8 °C) (Chen et al., 2017).

A large corpus of data show that T_a affected phenology (Wang and Engel, 1998; Lu et al., 2008) and normalized ATT (Tang et al., 2009; Zheng et al., 2014; Aslam et al., 2017). The ATT used here employ the Wang–Engel curvilinear temperature response function discussed elsewhere (Wang et al., 2017a), which showed an improved performance in modeling phenology. Recently, field experiments indicated that warming accelerated rice phenology depending on the warming level and pattern as shown in Fig. 4. For instance, all-day warming by 1.4–2.1 °C shortened the growth period by 1–5 d (Dong et al., 2011; Cai et al., 2016; Wang et al., 2018). The earlier end of the growing season of rice by 12 d was also reported under +4 °C all-day warming (Rani and Maragatham, 2013). Day-time warming by 1.1 °C and night-time warming by 0.5–1.8 °C also lead to 0–3 d early maturity (Dong et al., 2011; Chen et al., 2017). In addition, model findings indicated that growth duration of rice in China is shortened by 3–15 and 4.5–18 d, respectively, under +1.5 and +2.0 °C all-day warming scenarios at different sites (Liu et al., 2020). Our results support this consensus on rice growth duration for most of the seasons, where growth duration was shortened by 0–23 d, 0–14 d, 0–11 d and 1–16 d, respectively, under varying levels of all-day, day-time, night-time and asymmetric warming for cool season at different sites. However, for some warm seasons, our results showed that growth duration was prolonged by 0–4 d (Table 2) under differing warming patterns. Furthermore, the variation in growth duration under varying levels of warming are quasi-linear and decline with ambient seasonal mean T_a (Fig. 4, Table 3). Lu et al. (2008) also reported that seasonal mean T_a significantly affected the growth duration of rice, where a temperature increment of 1 °C resulted in shortened growth period of 4–5 d. Using 220 series of rice phenology in China covering the period of 1981–2006, it was shown that 95% of the series showed a negative correlation between the growth duration and seasonal mean T_a (Zhang et al., 2013).

The photoperiod also affects the phenology before the flowering stage (Lu et al., 2008; He et al., 2015). However, a previous study indicated that early and middle maturity rice is not sensitive to the photoperiod (Tang et al., 2009), which is the case for most of our datasets. For this reason, the photoperiod was not considered explicitly in the proposed model.

Combined with changes in growth duration, the effects of warming patterns on seasonal ET_c of rice were assessed. Changes in seasonal ET_c under varying levels of warming at all sites showed large variability with growing season, and generally reduced in cool season and slightly increased in warm season (Table 5). Prior model findings show inconsistent effects of all-day warming on seasonal ET_c as summarized in Table 7. The changes in seasonal ET_c under all-day warming here (Fig. 7) were within the range of values reported by Tao et al. (2008) (-18.2%–5.6%). These variations in seasonal ET_c under varying types of warming are attributed to the combined effects of changes in growth duration as earlier discussed and direct effects on ET_c. If no accounting for changes in growth duration is considered, the seasonal ET_c here differs in its response to various warming patterns (Table 5) depending on variation

in seasonal T_a and f_c (Figs. 6 and 7). Our results are also in line with reports for wheat production, in which the seasonal ET_c of wheat was increased by 18 mm under +3 °C all-day warming, whereas the overall ET_c was reduced when considering 13 days earlier crop mature (Asseng et al., 2004). To summarize, changed seasonal ET_c was shown to linearly or parabolically increase with increased ambient seasonal mean T_a under varying types of warming patterns (Fig. 7, Table 6). Not considering changes in growth duration can lead to negative correlations between changed seasonal ET_c and seasonal mean T_a under certain warming patterns (Fig. 7).

The modified P−T model can be used to estimate daily rice ET_c. At daily scale, the G was small and could be ignored Allen et al., 1998). Based on the pooled data from all sites (N=2093), a significant relation between daily R_n over rice field and daily R_s was found ($R_n = 0.638\ R_s$, with $R^2 = 0.91$) indicating that daily R_n over rice field could be estimated from daily R_s. Since the rice field was frequently flooded, no soil moisture constraints need to be accounted for. Hence, based on the Eqs. (1), ((2) and (16), the needed parameters of the modified P−T model are reduced to R_s and T_a, which are routinely provided in weather forecasts or from various climate models such as Coupled Model Intercomparison Project phase 5 (CMIP5) (Wang et al., 2017b). This reduced representation of daily rice ET_c and its implication for global rice production and water demands is kept for a future study.

Declaration of Competing Interest

The authors declare that they have no known competing financial interests or personal relationships that could have appeared to influence the work reported in this paper.

Acknowledgements

We sincerely appreciate the Asiaflux for their data collection and sharing efforts, Philippine Atmospheric, Geophysical, and Astronomical Services Administration (DOST-PAGASA) for providing the dataset in the Philippines and Dr. Mingzhong Zou for constructive comments and suggestions. We acknowledge the support from the National Natural Science Foundation of China (51509130, 51621061, 51822907), and the US National Science Foundation (NSF-AGS-1644382, NSF-IOS-1754893, and NSF-AGS-2028633).

Appendix

Fig A1

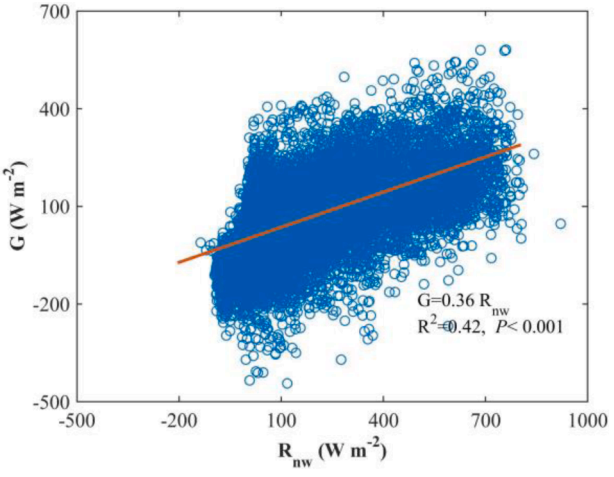

Fig A1.. Relation between surface soil heat flux (G) and net radiation received by the water or soil surface (R_{nw}) in paddy rice fields based on the pooled data.

References

Ai, Z., Yang, Y., 2016. Modification and validation of Priestley–Taylor model for estimating cotton evapotranspiration under plastic mulch condition. J. Hydrometeorol. 17 (4), 1281–1293.
Alberto, M.C.R., Hirano, T., Miyata, A., Wassmann, R., Kumar, A., Padre, A., Amante, M., 2012. Influence of climate variability on seasonal and interannual variations of ecosystem CO_2 exchange in flooded and non-flooded rice fields in the Philippines. Field Crops Res. 134 (3), 80–94.
Alberto, M.C.R., Wassmann, R., Buresh, R.J., Quilty, J.R., Jr, T.Q.C., Sandro, J.M., Centeno, C.A.R., 2014. Measuring methane flux from irrigated rice fields by eddy covariance method using open-path gas analyzer. Field Crops Res. 160 (4), 12–21.
Alberto, M.C.R., Wassmann, R., Hirano, T., Miyata, A., Hatano, R., Kumar, A., Padre, A., Amante, M., 2011. Comparisons of energy balance and evapotranspiration between flooded and aerobic rice fields in the Philippines. Agric. Water Manage. 98 (9), 1417–1430.
Alberto, M.C.R., Wassmann, R., Hirano, T., Miyata, A., Kumar, A., Padre, A., Amante, M., 2009. CO_2/heat fluxes in rice fields: Comparative assessment of flooded and non-flooded fields in the Philippines. Agric. For. Meteorol. 149 (10), 1737–1750.
Alexandratos, N., Bruinsma, J., 2012. World Agriculture: Towards 2030/2050 – The 2012 Revision. FAO, Rome. No. 12-03ESA working paper.
Allen, R.G., Pereira, L.S., 2009. Estimating crop coefficients from fraction of ground cover and height. Irrig. Sci. 28 (1), 17–34.
Allen, R.G., Pereira, L.S., Raes, D., Smith, M., 1998. Crop Evapotranspiration-Guidelines for Computing Crop Water Requirements. FAO, Rome, Italy. FAO Irrigation and Drainage Paper No. 56.
Aslam, M.A., Ahmed, M., Stöckle, C.O., Higgins, S.S., Hayat, R., 2017. Can growing degree days and photoperiod predict spring wheat phenology? Front. Environ. Sci. 5, 57.
Asseng, S., Jamieson, P.D., Kimball, B., Pinter, P., Sayre, K., Bowden, J.W., Howden, S. M., 2004. Simulated wheat growth affected by rising temperature, increased water deficit and elevated atmospheric CO_2. Field Crops Res. 85 (2), 85–102.
Cai, C., Yin, X.Y., He, S.Q., Jiang, W.Y., Si, C.F., Struik, P.C., Luo, W.H., Li, G., Xie, Y.T., Xiong, Y., Pan, G.X., 2016. Responses of wheat and rice to factorial combinations of ambient and elevated CO_2 and temperature in FACE experiments. Global Change Biol. 22 (2), 856–874.
Choudhury, B.J., Idso, S.B., Reginato, R.J., 1987. Analysis of an empirical model for soil heat flux under a growing wheat crop for estimating evaporation by an infrared-temperature based energy balance equation. Agric. For. Meteorol. 39 (4), 283–297.
Chen, J., Chen, C.G., Tian, Y.L., Zhang, X., Dong, W.J., Zhang, B., Zhang, J., Zheng, C.Y., Deng, A.X., Song, Z.W., Zhang, W.J., 2017. Differences in the impacts of night-time warming on crop growth of rice-based cropping systems under field conditions. Eur. J. Agron. 82, 80–92.
Ding, R.S., Kang, S.Z., Li, F.S., Zhang, Y.Q., Tong, L., 2013a. Evapotranspiration measurement and estimation using modified Priestley–Taylor model in an irrigated maize field with mulching. Agric. For. Meteorol. 168, 140–148.
Ding, R.S., Kang, S.Z., Li, F.S., Zhang, Y.Q., Tong, L., Sun, Q.Y., 2010. Evaluating eddy covariance method by large-scale weighing lysimeter in a maize field of northwest China. Agric. Water Manage. 98 (1), 87–95.
Ding, R.S., Kang, S.Z., Zhang, Y.Q., Hao, X.M., Tong, L., Du, T.S., 2013b. Partitioning evapotranspiration into soil evaporation and transpiration using a modified dual crop coefficient model in irrigated maize field with ground-mulching. Agric. Water Manage. 127, 85–96.
Dong, W.J., Chen, J., Zhang, B., Tian, Y.L., Zhang, W.J., 2011. Responses of biomass growth and grain yield of midseason rice to the anticipated warming with FATI facility in East China. Field Crops Res. 123 (3), 259–265.
Ershadi, A., McCabe, M.F., Evans, J.P., Chaney, N.W., Wood, E.F., 2014. Multi-site evaluation of terrestrial evaporation models using FLUXNET data. Agric. For. Meteorol. 187, 46–61.
FAO, 2020. Food and Agricultural Organization (online report): Land and Water Section http://www.fao.org/faostat/en/#data/QC, accessed: 2020-04-16.
Fisher, J.B., Tu, K.P., Baldocchi, D.D., 2008. Global estimates of the land–atmosphere water flux based on monthly AVHRR and ISLSCP-II data, validated at 16 FLUXNET sites. Remote Sens. Environ. 112 (3), 901–919.
Godfray, H.C.J., Beddington, J.R., Crute, I.R., Haddad, L., Lawrence, D., Muir, J.F., Pretty, J., Robinson, S., Thomas, S.M., Toulmin, C., 2010. Food security: the challenge of feeding 9 billion people. Science 327 (5967), 812–818.
Gong, X.W., Qiu, R.J., Ge, J.K., Bo, G.K., Ping, Y.L., Xin, Q.S., Wang, S.S., 2021. Evapotranspiration partitioning of greenhouse grown tomato using a modified Priestley-Taylor model. Agric. Water Manage. https://doi.org/10.1016/j.agwat.2020.106709. In press.
He, L., Asseng, S., Zhao, G., Wu, D.R., Yang, X.Y., Zhuang, W., Jin, N., Yu, Q., 2015. Impacts of recent climate warming, cultivar changes, and crop management on winter wheat phenology across the Loess Plateau of China. Agric. For. Meteorol. 200, 135–143.
Core Writing Team IPCC, 2014. Climate change 2014: synthesis report. In: Pachauri, R. K., Meyer, L.A. (Eds.), Contribution of Working Groups I, II and III to the fifth assessment report of the Intergovernmental Panel on Climate Change. Geneva, Switzerland. IPCC. Core Writing Team.
Kim, H., Ko, J., Kang, S., Tenhunen, J., 2013. Impacts of climate change on paddy rice yield in a temperate climate. Global Change Biol. 19 (2), 548–562.
Koster, R.D., Sud, Y.C., Guo, Z., Dirmeyer, P.A., Bonan, G., Oleson, K.W., Chan, E., Verseghy, D., Cox, P., Davies, H., Xue, Y., 2006. GLACE: the global land–atmosphere coupling experiment. Part I: Overview. J. Hydrometeorol. 7 (4), 590–610.
Liu, C.W., Kang, S.Z., Li, F.S., Li, S.E., Du, T.S., 2013. Canopy leaf area index for apple tree using hemispherical photography in arid region. Sci. Hortic. 164, 610–615.

Liu, X.Y., Xu, J.Z., Yang, S.H., Zhang, J.G., 2018. Rice evapotranspiration at the field and canopy scales under water-saving irrigation. Meteorol. Atmos. Phys. 130 (2), 227–240.
Liu, Y.J., Tang, L., Qiu, X.L., Liu, B., Chang, X.N., Liu, L.L., Zhang, X.H., Cao, W.X., Zhu, Y., 2020. Impacts of 1.5 and 2.0°C global warming on rice production across China. Agric. For. Meteorol. 284, 107900.
Lu, P.L., Yu, Q., Wang, E.L., Liu, J.D., Xu, S.H., 2008. Effects of climatic variation and warming on rice development across South China. Clim. Res. 36 (1), 79–88.
Lv, Y.P., Xu, J.Z., Yang, S.H., Liu, X.Y., Zhang, J.G., Wang, Y.J., 2018. Inter-seasonal and cross-treatment variability in single-crop coefficients for rice evapotranspiration estimation and their validation under drying-wetting cycle conditions. Agric. Water Manage. 196, 154–161.
Ma, X.Y., Zhou, G.S., 2013. Method of determining the maximum leaf area index of spring maize and its application. Acta Ecol. Sinica 33 (8), 2596–2603.
Mahmood, R., 1997. Impacts of air temperature variations on the boro rice phenology in Bangladesh: implications for irrigation requirements. Agric. For. Meteorol. 84 (3), 233–247.
Morgan, C.L., Norman, J.M., Lowery, B., 2003. Estimating plant-available water across a field with an inverse yield model. Soil Sci. Soc. Am. J. 67 (2), 620–629.
Ono, K., Mano, M., Han, G.H., Nagai, H., Yamada, T., Kobayashi, Y., Miyata, A., Inoue, Y., Lal, R., 2015. Environmental controls on fallow carbon dioxide flux in a single-crop rice paddy, Japan. Land Degrad. Dev. 26 (4), 331–339.
Pan, S.F., Tian, H.Q., Dangal, S.R.S., Yang, Q.C., Yang, J., Lu, C.Q., Tao, B., Ren, W., Ouyang, Z., 2015. Responses of global terrestrial evapotranspiration to climate change and increasing atmospheric CO2 in the 21st century. Earth's Future 3 (1), 15–35.
Paredes, P., Pereira, L.S., 2019. Computing FAO56 reference grass evapotranspiration PM-ETo from temperature with focus on solar radiation. Agric. Water Manage. 215, 86–102.
Peng, S.B., Huang, J.L., Sheehy, J.E., Laza, R.C., Visperas, R.M., Zhong, X.H., Centeno, G. S., Khush, G.S., Cassman, K.G., 2004. Rice yields decline with higher night temperature from global warming. Proc. Natl. Acad. Sci. U. S. A. 101 (27), 9971–9975.
Priestley, C.H.B., Taylor, R.J., 1972. On the assessment of surface heat flux and evaporation using large-scale parameters. Mon. Weather Rev. 100 (2), 81–92.
Qiu, R.J., Du, T.S., Kang, S.Z., Chen, R.Q., Wu, L.S., 2015. Assessing the SIMDualKc model for estimating evapotranspiration of hot pepper grown in a solar greenhouse in Northwest China. Agric. Syst. 138, 1–9.
Qiu, R.J., Li, L.A., Kang, S.Z., Liu, C.W., Wang, Z.C., Cajucom, P.E., Zhang, B.Z., Agathokleous, E., 2021. An improved method to estimate actual vapor pressure without relative humidity data. Agric. For. Meteorol. In press.
Qiu, R.J., Liu, C.W., Cui, N.B., Wu, Y.J., Wang, Z.C., Li, G., 2019. Evapotranspiration estimation using a modified Priestley-Taylor model in a rice-wheat rotation system. Agric. Water Manage. 224, 105755.
Rani, B.A., Maragatham, N., 2013. Effects of elevated temperature on rice phenology and yield. Inidan J. Sci. Technol. 6 (8), 5095–5097.
Saito, M., Miyata, A., Nagai, H., Yamada, T., 2005. Seasonal variation of carbon dioxide exchange in rice paddy field in Japan. Agric. For. Meteorol. 135 (1), 93–109.
Sánchez, B., Rasmussen, A., Porter, J.R., 2014. Temperatures and the growth and development of maize and rice: a review. Global Change Biol. 20 (2), 408–417.
Saptomo, S.K., Setiawan, B.I., Yuge, K., 2009. Climate change effects on paddy field thermal environment and evapotranspiration. Paddy Water Environ. 7 (4), 341.
Schaap, M.G., 1999. Rosetta Lite Version 1.0. Predicting Soil Hydraulic Parameters from Basic Data. U.S. Salinity Laboratory, USDA/ARS, Riverside, CA.
Seck, P.A., Diagne, A., Mohanty, S., Wopereis, M.C.S., 2012. Crops that feed the world 7: Rice. Food Secur. 4 (1), 7–24.
Steduto, P., Hsiao, T.C., Raes, D., Fereres, E., 2009. AquaCrop—the FAO crop model to simulate yield response to water: I. Concepts and underlying principles. Agron. J. 101 (3), 426–437.
Sumner, D.M., Jacobs, J.M., 2005. Utility of Penman–Monteith, Priestley–Taylor, reference evapotranspiration, and pan evaporation methods to estimate pasture evapotranspiration. J. Hydrol. 308 (1–4), 81–104.
Tang, L., Zhu, Y., Hannaway, D., Meng, Y., Liu, L., Chen, L., Cao, W., 2009. RiceGrow: a rice growth and productivity model. NJAS 57 (1), 83–92.
Tanner, C.B., Jury, W.A., 1976. Estimating evaporation and transpiration from a row cop during incomplete cover. Agron. J. 68 (2), 239–243.
Tao, F.L., Hayashi, Y., Zhang, Z., Sakamoto, T., Yokozawa, M., 2008. Global warming, rice production, and water use in China: Developing a probabilistic assessment. Agric. For. Meteorol. 148 (1), 94–110.
Todorovic, M., Karic, B., Pereira, L.S., 2013. Reference evapotranspiration estimate with limited weather data across a range of Mediterranean climates. J. Hydrol. 481, 166–176.
Twine, T.E., Kustas, W.P., Norman, J.M., Cook, D.R., Houser, P.R., Meyers, T.P., Prueger, J.H., Starks, P.J., Wesely, M.L., 2000. Correcting eddy-covariance flux underestimates over a grassland. Agric. For. Meteorol. 103 (3), 279–300.
Wang, B., Li, J.L., Wan, Y.F., Cai, W.W., Guo, C., You, S.C., Li, R.N., Qin, X.B., Gao, Q.Z., Zhou, S.H., Li, Y.E., 2019. Variable effects of 2°C air warming on yield formation under elevated [CO2] in a Chinese double rice cropping system. Agric. For. Meteorol. 278, 107662.
Wang, E.L., Engel, T., 1998. Simulation of phenological development of wheat crops. Agric. Syst. 58 (1), 1–24.
Wang, E.L., Martre, P., Zhao, Z.G., Ewert, F., Maiorano, A., Rötter, R.P., Kimball, B.A., Ottman, M.J., Wall, G.W., White, J.W., 2017a. The uncertainty of crop yield projections is reduced by improved temperature response functions. Nat. Plants 3 (8), 1–13.
Wang, K.C., Dickinson, R.E., 2012. A review of global terrestrial evapotranspiration: observation, modeling, climatology, and climatic variability. Rev. Geophys. 50 (2), RG2005.
Wang, W.G., Ding, Y.M., Shao, Q.X., Xu, J.Z., Jiao, X.Y., Luo, Y.F., Yu, Z.B., 2017b. Bayesian multi-model projection of irrigation requirement and water use efficiency in three typical rice plantation region of China based on CMIP5. Agric. For. Meteorol. 232, 89–105.
Wang, W.L., Cai, C., Lam, S.K., Liu, G., Zhu, J.G., 2018. Elevated CO_2 cannot compensate for japonica grain yield losses under increasing air temperature because of the decrease in spikelet density. Eur. J. Agron. 99, 21–29.
Xu, J.Z., Bai, W.H., Li, Y.W., Wang, H.Y., Yang, S.H., Wei, Z., 2019. Modeling rice development and field water balance using AquaCrop model under drying-wetting cycle condition in eastern China. Agric. Water Manage. 213, 289–297.
Xu, J.Z., Liu, X.Y., Yang, S.H., Qi, Z.M., Wang, Y.I., 2017a. Modeling rice evapotranspiration under water-saving irrigation by calibrating canopy resistance model parameters in the Penman-Monteith equation. Agric. Water Manage. 182, 55–66.
Xu, J.Z., Lv, Y.P., Ai, L.K., Yang, S.H., He, Y.P., Dalson, T., 2017b. Validation of dual-crop coefficient method for calculation of rice evapotranspiration under drying–wetting cycle condition. Paddy Water Environ. 15 (2), 381–393.
Yao, Y., Liang, S., Cheng, J., Liu, S., Fisher, J.B., Zhang, X., Jia, K., Zhao, X., Qin, Q., Zhao, B., 2013. MODIS-driven estimation of terrestrial latent heat flux in China based on a modified Priestley–Taylor algorithm. Agric. For. Meteorol. 171, 187–202.
Zhang, Q., Yang, Z.S., Hao, X.C., Yue, P., 2019. Conversion features of evapotranspiration responding to climate warming in transitional climate regions in northern China. Clim. Dyn. 52 (7), 3891–3903.
Zhang, T.Y., Huang, Y., Yang, X.G., 2013. Climate warming over the past three decades has shortened rice growth duration in China and cultivar shifts have further accelerated the process for late rice. Global Change Biol. 19 (2), 563–570.
Zheng, B.Y., Chenu, K., Doherty, A. and Chapman, S., 2014. The APSIM-Wheat Module (7.5 R3008). Agricultural production systems simulator (APSIM) initiative, Toowoomba, Australian.